Stability analysis of VSC based on SISO equivalent in current control time scale

*Yaxin Peng, Xiaoming Yuan

2020 IEEE 1st China International Youth Conference on Electrical Engineering (CIYCEE) | 978-1-7281-9659-6/20/$31.00 ©2020 IEEE | DOI: 10.1109/CIYCEE49808.2020.9332602

***Abstract* - Oscillations in current control (CC) timescale (higher than 50 Hz) caused by voltage source converters (VSCs) integrating into the weak grid have occurred. However, relevant studies lack enough mechanism cognitions of instability of such system. In order to guide the parameter setting of the controllers, this paper first presents a small signal model of VSC based on motion equation concept. Secondly, a SISO equivalent method which can quantitatively analyze the interaction between variables in MIMO is introduced. Thirdly, the influence of phase locked loop (PLL) bandwidth, current controller parameters in the *d-axis* and *q*-axis and filter bandwidth on the feedforward branch of terminal voltage on stability is analyzed based the SISO equivalent method, which can help engineers to study the mechanisms of the voltage amplitude/frequency stability. Finally, the simulations in time domain verify the correctness of the analyses.**

***Index Terms*-- current control (CC) timescale, voltage source converter (VSC), SISO equivalent, stability analysis**

I. INTRODUCTION

DRIVEN by environmental protection, power electronic technology progress and other factors, power electronic to be dominated is an inevitable trend of power system development [1]. The VSC is widely used in wind power generation, photovoltaic power generation and other fields because of its flexible and controllable characteristics. In CC timescale, the problem of high frequency oscillations caused by VSC when integrating into the weak grid has attracted attention [2]. Many scholars have done a lot of research on this problem. The researches can be summarized as eigenvalue analysis method and impedance analysis method.

Eigenvalue analysis method [3] is a time domain analysis method based on state space model, which can accurately judge the stability of the system according to the eigenvalue. Some useful information such as participation factor and sensitivity can be derived. However, the analysis relying on specific scenarios lacks mechanism cognition and is difficult to be applied to large-scale system.

Impedance analysis is a frequency domain analysis method based on small signal model, which is widely used. According to the different coordinate systems used in modeling, impedance analysis methods can be roughly divided into three categories: the first category is the sequence-domain impedance models established in $\alpha\beta$ coordinate [4], [5], the second category is the impedance model established in dq coordinate [6], and the third category is the generalized impedance model [7] with amplitude and phase as input and output signal in polar coordinates. For the three-phase converter grid connected system, the two-dimensional impedance matrix has coupling characteristics when considering the PLL dynamic or current controller structure or parameter asymmetry, and there is no special symmetrical structure. The generalized Nyquist criterion which is difficult to reflect the stability margin are usually used. Or it is considered that the system matrix is approximately decoupled through some assumptions and can be equivalent to two SISO systems, thus, the universality is limited. What's more, equipment and network are regarded as black box, which limits the mechanism analysis of system dynamic problems to a certain extent.

The core goal of power system is to ensure the balance of supply and demand of active and reactive power, and maintain the voltage's amplitude and frequency in a reasonable range. The equipment model based on motion equation concept can be used to describe the dynamic process of the internal voltage's amplitude and frequency driven by unbalanced active and reactive power, and has been widely used to analyze the dynamic characteristics of diversified equipment. The concept of motion equation in CC time scale refers to the amplitude and frequency motion of VSC's internal voltage driven by active/reactive reference currents and active/reactive feedback currents [8]. The model is derived basing on physical understanding of equipment's abstract function rather than on the structure of the equipment, which can reflect the mechanism of the dynamic process of the system. Literature [8] established a small signal model of VSC based motion equation model without considering terminal voltage feedforward and current controller parameters asymmetry in dq axis. Considering the complexity of MIMO system analysis and in order to have a more comprehensive understanding of the influence mechanism of parameter changes on stability, this paper establishes a small signal model of VSC considering phase locked loop's dynamics, controller parameter asymmetry in dq axis and terminal voltage feedforward based on motion equation concept in CC time-scale. And then stability analysis is carried out based on a SISO equivalent method that can analyze the interaction between different MIMO's variables.

The rest of paper is organized as follows. Section II presents a small signal model of VSC based motion equation concept. Section III introduces the SISO equivalent method of MIMO system. Section IV analyzes the influence of PLL bandwidth, current controller parameters in dq axis and filter bandwidth on the stability of the VSC grid-connected system. Section V draw the conclusions.

II. SMALL SIGNAL MODELING OF SYSTEM

A. Small Signal Model of VSC

The basic topology and control structure diagram of VSC are described in Fig.1. The current control strategy adopts double PI control based on PLL, and considers terminal voltage feedforward and the current cross decoupling term. The red part shows a typical second-order PLL, which can track the position of the terminal voltage and realize the synchronization between converter and grid. L_f is filter

This work was supported in part by the Joint fund Program of National Natural Science Fund of China under Grant U1766202.

The authors are with the State Key Laboratory of Advanced Electromagnetic Engineering and Technology, and School of Electrical and Electronic Engineering, Huazhong University of Science and Technology, Wuhan 430074, China (e-mail: pengyaxin@hust.edu.cn).

inductance, L_g is the equivalent inductance of the grid. A damping resistor R_c is connected in series with the filter capacitor C_f to suppress the resonance caused by LC filter. In Fig. 1, $\boldsymbol{e}$ represents the internal voltage vector in VSC, $\boldsymbol{i}_{\text{ref}}$ and $\boldsymbol{i}$ represent the command current vector and feedback current vector respectively, $\boldsymbol{u_t}$ is the terminal voltage vector. E,θ_e,ω_e,is the amplitude, phase and frequency of the internal voltage, and the subscripts dq^p, dq^e,$\alpha\beta$ denote the variables in rotating PLL-synchronized coordinate, rotating dq coordinate with the vector $\boldsymbol{e}$ oriented, and in the static coordinate. The position relationships between different coordinate and vectors are shown in Fig. 2, where xy coordinate is coordinate with terminal voltage in steady state $\boldsymbol{u_t}$ oriented and rotate at synchronous speed ω_0 It should be noted that current controller is operated in dq coordinate, as long as the position of PLL and terminal voltage is different, i_d^p and i_q^p is no longer the actual active and reactive current relative to terminal voltage.

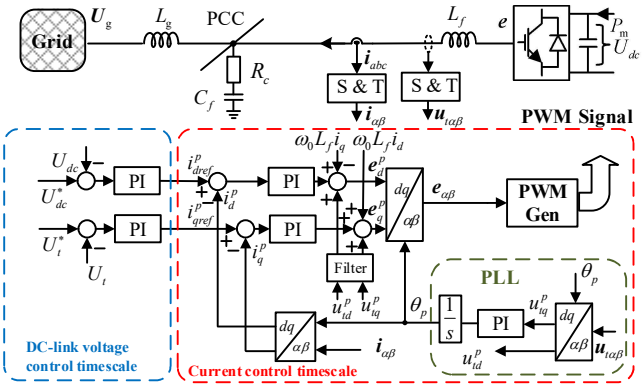

Fig. 1. Basic topology and control structure diagram of VSC

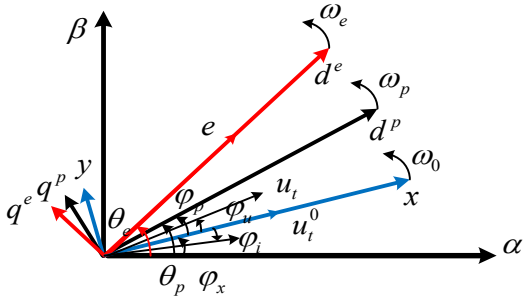

Fig. 2. The position relationship between different coordinates and vectors

This paper does not pay attention to high-frequency oscillation caused by LCL filter. Therefore, average value model is adopted and the effect of delay is neglected. To simplify the analysis, the following assumptions are made: (1) Reference currents i_{dref}^p, i_{qref}^p are supposed to keep constant; (2) Losses of inductance resistances are ignored.

Based on the motion equation concept, to obtain the small signal model of VSC with actual unbalanced active/reactive current as input signal and amplitude/frequency as output signal, the basic control structure of VSC in CC time scale shown in Fig.1. can be transformed into Fig. 3 (a). Where $\boldsymbol{i}_{dq}^e$, $\boldsymbol{i}_{dqref}^e$ are active/reactive feedback current and active/reactive reference current relative to internal voltage; $\varepsilon\boldsymbol{i}_{dq}^e = \boldsymbol{i}_{dqref}^e - \boldsymbol{i}_{dq}^e$ are unbalanced active/reactive current. $\mathbf{G_c(s)}$ is the current controller, $\mathbf{F_v(s)}$ is low-pass filter. The expression is as follows.

$$\mathbf{G_c(s)}=\begin{bmatrix} G_{cd}(s) & \omega_0 L_f \\ -\omega_0 L_f & G_{cq}(s) \end{bmatrix} \quad \begin{aligned} G_{cd}(s)&=k_{pcd}+\frac{k_{icd}}{s} \\ G_{cq}(s)&=k_{pcq}+\frac{k_{icq}}{s} \end{aligned} \tag{1}$$

$$\mathbf{F_v(s)}=\begin{bmatrix} F_v(s) & 0 \\ 0 & F_v(s) \end{bmatrix} \quad F_v(s)=\frac{a_{fv}}{s+a_{fv}} \tag{2}$$

Where k_{pcd}, k_{pcq}, k_{icd}, k_{icq} are the proportional and integral parameters of PI current controller in dq axis respectively; a_{fv} is the cut-off frequency of the low-pass filter.

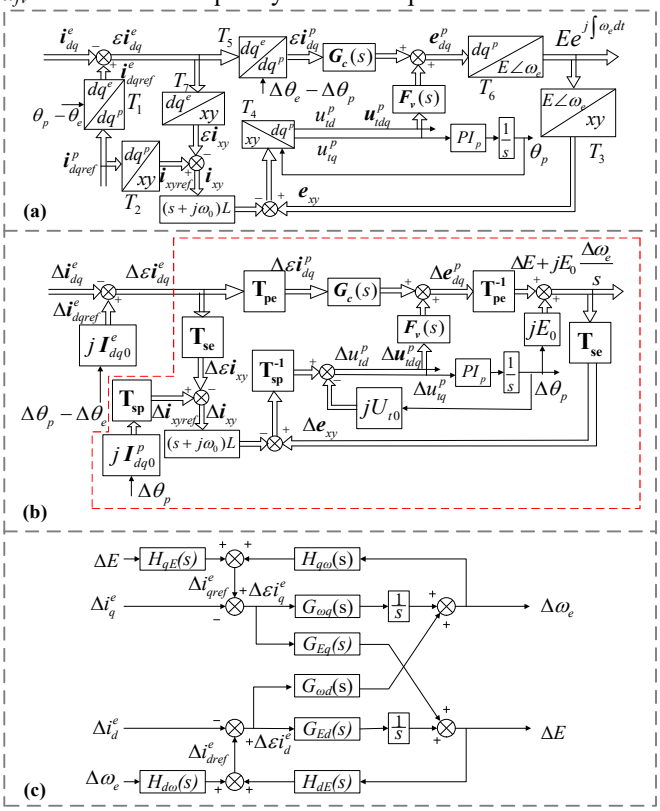

Fig. 3. Modeling process of VSC in CC timescale

The nonlinear part in Fig. 3 (a) is mainly reflected in the coordinate transformation. Therefore, the coordinate transformation is linearized and the results are as follows. Where the subscript 0 represents the steady-state value.

T_1: $\Delta \boldsymbol{i}_{dqref}^e = jI_{dq}^e(\Delta\theta_p - \Delta\theta_e)$

$$T_2:\begin{bmatrix}\Delta i_{xref}\\ \Delta i_{yref}\end{bmatrix}=\mathbf{T_{sp}}\begin{bmatrix}-I_{q0}^p\\ I_{d0}^p\end{bmatrix}\Delta\theta_p \qquad T_3:\begin{bmatrix}\Delta e_x\\ \Delta e_y\end{bmatrix}=\mathbf{T_{se}}\begin{bmatrix}\Delta E\\ E_0\dfrac{\Delta\omega_e}{s}\end{bmatrix}$$

$$T_4:\begin{bmatrix}\Delta u_{td}^p\\ \Delta u_{tq}^p\end{bmatrix}=\mathbf{T_{sp}^{-1}}\begin{bmatrix}\Delta u_{tx}\\ \Delta u_{ty}\end{bmatrix}-\begin{bmatrix}0\\ U_{t0}\end{bmatrix}\Delta\theta_p \quad T_5:\begin{bmatrix}\Delta\varepsilon i_d^p\\ \Delta\varepsilon i_q^p\end{bmatrix}=\mathbf{T_{pe}}\begin{bmatrix}\Delta\varepsilon i_d^e\\ \Delta\varepsilon i_q^e\end{bmatrix} \tag{3}$$

$$T_6:\begin{bmatrix}\Delta E\\ E_0\dfrac{\Delta\omega_e}{s}\end{bmatrix}=\mathbf{T_{pe}^{-1}}\begin{bmatrix}\Delta e_d^p\\ \Delta e_q^p\end{bmatrix}+\begin{bmatrix}0\\ E_0\end{bmatrix}\Delta\theta_p \; T_7:\begin{bmatrix}\Delta\varepsilon i_x\\ \Delta\varepsilon i_y\end{bmatrix}=\mathbf{T_{se}}\begin{bmatrix}\Delta\varepsilon i_d^e\\ \Delta\varepsilon i_q^e\end{bmatrix}$$

where

$$\mathbf{T_{sp}}=\begin{bmatrix}cos\varphi_p & -sin\varphi_p\\ sin\varphi_p & cos\varphi_p\end{bmatrix}\mathbf{T_{se}}=\begin{bmatrix}cos\varphi_e & -sin\varphi_e\\ sin\varphi_e & cos\varphi_e\end{bmatrix}\mathbf{T_{pe}}=\mathbf{T_{se}}\mathbf{T_{sp}^{-1}}$$

Terminal voltage can be obtained from the internal voltage and feedback current, i.e

$$\begin{bmatrix}u_{tx}\\ u_{ty}\end{bmatrix}=\begin{bmatrix}e_x\\ e_y\end{bmatrix}-\begin{bmatrix}sL_f & \omega_0 L_f\\ -\omega_0 L_f & sL_f\end{bmatrix}\begin{bmatrix}i_x\\ i_y\end{bmatrix} \tag{3}$$

The transfer function of PLL is as follows:

$$\Delta\theta_p = G_p(s)\Delta u_{tq}^p \qquad G_p(s)=\frac{k_{pp}s+k_{ip}}{s} \tag{4}$$

Where k_{pp} and k_{ip} are the proportional and integral parameters of the PI controller of PLL respectively. The red

part in Fig. 3 (b) which shows the linearized model can be used to obtain transfer function from $\Delta\varepsilon\boldsymbol{i}^e_{dq}$ to $\Delta\theta_p$,which is as follows.

$$\Delta\theta_p = G_{dpll}(s)\Delta\varepsilon i^e_d + G_{qpll}(s)\Delta\varepsilon i^e_q \tag{5}$$

Associate (1)(2)(3)(6) and Fig.3(b), transfer function from $\Delta\varepsilon\boldsymbol{i}^e_{dq}$ to ΔE, $\Delta\omega_e$ can be derived as follows.

$$\begin{bmatrix}\Delta E\\ \Delta\omega_e\end{bmatrix} = \begin{bmatrix}G_{Ed}(s)/s & G_{Eq}(s)\\ G_{\omega d}(s) & G_{\omega q}(s)/s\end{bmatrix}\begin{bmatrix}\Delta\varepsilon i^e_d\\ \Delta\varepsilon i^e_q\end{bmatrix} \tag{6}$$

Associate (6)(7) transfer function from ΔE, $\Delta\omega_e$ to $\Delta\theta_p$ can be derived as follows.

$$\Delta\theta_p = G_{Epll}(s)\Delta E + G_{\omega pll}(s)\Delta\omega_e \tag{7}$$

Associate (4)(8) transfer function from ΔE, $\Delta\omega_e$ to Δi^e_{dref}, Δi^e_{qref} can be derived as follows.

$$\begin{bmatrix}\Delta i^e_{dref}\\ \Delta i^e_{qref}\end{bmatrix} = \begin{bmatrix}H_{dE}(s) & H_{d\omega}(s)\\ H_{qE}(s) & H_{q\omega}(s)\end{bmatrix}\begin{bmatrix}\Delta E\\ \Delta\omega_e\end{bmatrix} \tag{8}$$

Associate (7)(9), small signal model of VSC can be derived in Fig.3(c). The specific expressions are shown in appendix.

B. Small Signal of Grid

Since internal voltage's amplitude/frequency is the response driven by unbalanced active and reactive current in equipment model, it is necessary to obtain the grid's small signal model with the internal voltage amplitude frequency as input signal and feedback active and reactive current as output signal. The transfer function of grid shown in Fig. 1 in *xy* coordinate is as follows:

$$Y(s+j\omega_0) = Y_x(s) + jY_y(s) = \frac{\Delta i_{xy}}{\Delta e_{xy}} \tag{10}$$

$$= \frac{L_gC_f(s+j\omega_0)^2 + R_cC_f(s+j\omega_0)+1}{L_gC_fL_f(s+j\omega_0)^3 + R_cC_f(L_g+L_f)(s+j\omega_0)^2 + (L_g+L_f)(s+j\omega_0)}$$

Where

$$\begin{aligned}Y_x(s) &= \left[Y(s+j\omega_0)+Y(s-j\omega_0)\right]/2\\ Y_y(s) &= \left[Y(s+j\omega_0)-Y(s-j\omega_0)\right]/2j\end{aligned} \tag{9}$$

From (4) we know,

$$\begin{bmatrix}\Delta e_x\\ \Delta e_y\end{bmatrix} = \mathbf{T_{se}}\begin{bmatrix}\Delta E\\ E_0\dfrac{\Delta\omega_e}{s}\end{bmatrix} \quad \begin{bmatrix}\Delta i^e_d\\ \Delta i^e_q\end{bmatrix} = \mathbf{T_{se}}^{-1}\begin{bmatrix}\Delta i_x\\ \Delta i_y\end{bmatrix} - \begin{bmatrix}-I^e_{q0}\\ I^e_{d0}\end{bmatrix}\Delta\theta_e \tag{10}$$

Thus, the small signal model of the network can be obtained as follows:

$$\begin{bmatrix}\Delta i^e_d\\ \Delta i^e_q\end{bmatrix} = \begin{bmatrix}\underbrace{Y_x(s)}_{H_{11}(s)} & \underbrace{\left(-E_0Y_y(s)+I^e_{q0}\right)/s}_{H_{12}(s)}\\ \underbrace{Y_y(s)}_{H_{21}(s)} & \underbrace{\left(-E_0Y_x(s)-I^e_{d0}\right)/s}_{H_{22}(s)}\end{bmatrix}\begin{bmatrix}\Delta E\\ \Delta\omega_e\end{bmatrix} \tag{11}$$

Combined with the small signal model of VSC, the small signal model of the system can be obtained in Fig.4.

III. INTRODUCTION OF SISO EQUIVALENT METHOD

When considering the influence of PLL's dynamic and asymmetric parameters in *dq* axis controller, it is difficult to decouple the equipment and network model at the same time.

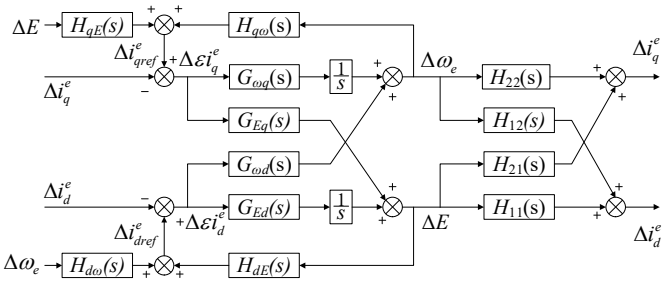

Fig. 4. The frequency domain model of the single VSC and infinite bus system depicted in Fig. 1.

The system model is MIMO with strong coupling characteristics. However, the existing generalized Nyquist criteria and norm criteria can only judge the stability, but cannot reflect the stability margin. The analysis of SISO system is simpler than MIMO system, the technology is more mature, and it is easy to quantify the system stability margin. To quantitatively analyze the interaction between different variables, the equivalent SISO system needs to retain the interaction path between variables in MIMO system. Taking small signal model of single VSC and infinite bus system in Fig. 4 as an example, this paper introduces an equivalent SISO method that preserves the interaction path between key variables [9]. It should be noted that the SISO equivalent method can only be used when MIMO linear autonomous system has no external input.

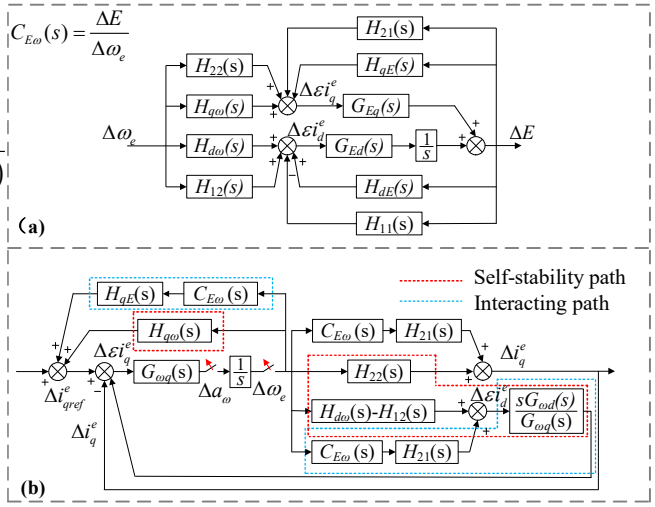

Fig. 5. The process of SISO equivalent of MIMO system

(1) Determine the key state variables that need to be retained in MIMO system, such as ΔE, $\Delta\omega_e$, then select one of them such as $\Delta\omega_e$ as the research object, and open its loop.

(2) As shown in Fig. 5 (a), the open-loop transfer function $C_{E\omega}(s)$ from research object $\Delta\omega_e$ to other key state variables ΔE is obtained. The specific expression is shown in appendix.

(3) Calculate the influence of other key state variables on the relevant input of the research object combined with (2), the input variation of the research object caused by other key state variables can be transformed into the dynamic of the research object itself. So that the interaction between key state variables can be equivalent to the dynamic of the research object itself, such as the blue part in Fig. 5 (b), which is called the interacting path. It should be noted that the amplitude and frequency also interact with each other through the internal coupling channel $G_{\omega d}(s)$ of VSC, which can be equivalent to amplitude dynamics affect frequency

dynamics by influencing unbalanced reactive current.

(4) Calculate the input variation caused by the research object itself, such as the red part in Fig. 5 (b), which is the self-stability path. Combining with (3), and then closing the loop of research object, the equivalent SISO can be obtained.

IV. SISO EQUIVALENT BASED STABILITY ANALYSIS

Except the Nyquist criterion, the stability criterion proposed in literature [10] can not only judge the stability, but also quantitatively analyze the influence of interaction between variables on stability. In most cases, change rate of amplitude and frequency will be retained in the small signal model of system. Combined with the above stability criterion and the typical structure of equivalent SISO system after retaining the change rate in Fig. 6, the stability criteria of the system can be modified as follows.

Obviously, the system's characteristic polynomial is $T(s)=s-D(s)$, let $s=j\omega$ and the oscillation frequency of the system ω_m can be approximately estimated by $\mathrm{Im}[T(j\omega)]=0$, that is, $\omega-\mathrm{Im}[D(j\omega)]=0$.

(1) When the slope of $\omega-\mathrm{Im}[D(j\omega)]$ at ω_m is greater than 0, if $\mathrm{Re}[D(j\omega_m)]\leq 0$ the system is stable, otherwise the system is unstable.

(2) When the slope of $\omega-\mathrm{Im}[D(j\omega)]$ at ω_m is less than 0, if $\mathrm{Re}[D(j\omega_m)]\geq 0$, the system is stable, otherwise the system is unstable.

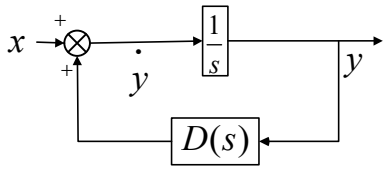

Fig. 6. The typical structure of equivalent SISO system after retaining the change rate

If the characteristic polynomial $T(j\omega)$ is decomposed according to the division of path in section III, the contribution of different paths to stability can be quantitatively analyzed according to the positive and negative and relative size of $\mathrm{Re}[T(j\omega_m)]$.

Any variable's stability can reflect system's stability, so the equivalent SISO system obtained by selecting different research objects both can reflect the original MIMO system's stability. This paper only focuses on the frequency dynamic, and takes the frequency as the research object to analyze the equivalent SISO system shown in Fig. 5. Disconnect the SISO system as shown in Fig. 5, we can get equation (14).

$$
\begin{aligned}
&D_\omega(s)=\frac{\Delta a_\omega}{\Delta\omega_e}=D_{self\omega}(s)+D_{enE}(s)\\
&D_{self\omega}(s)=\underbrace{G_{\omega q}(s)\left[H_{q\omega}(s)-H_{22}(s)\right]}_{D_{self1\omega}(s)}+\underbrace{sG_{\omega d}(s)\left[H_{d\omega}(s)-H_{12}(s)\right]}_{D_{self2\omega}(s)}\\
&D_{enE}(s)=\underbrace{C_{E\omega}(s)G_{\omega q}(s)\left[H_{qE}(s)-H_{21}(s)\right]}_{D_{en1E}(s)} \qquad (14)\\
&\quad+\underbrace{sC_{E\omega}(s)G_{\omega d}(s)\left[H_{dE}(s)-H_{11}(s)\right]}_{D_{en2E}(s)}
\end{aligned}
$$

$D_\omega(s)$ can be used to analyze the frequency stability of the system. $D_{self\omega}(s)$ is the self-stability path, which is used to analyze the influence of frequency dynamics on its own stability. The self-stability path can be divided into two parts: $D_{self1\omega}(s)$ determined by branch from unbalanced reactive current to frequency (below referred to as main branch) and $D_{self2\omega}(s)$ determined by coupling branch from unbalanced active/reactive current to amplitude/frequency in equipment. $D_{enE}(s)$ is the interacting path, which is used to analyze the influence of the interaction between amplitude dynamic and frequency dynamic on frequency stability. The interacting stability path can be divided into two parts: $D_{en1E}(s)$ determined by unbalanced reactive current to frequency branch, and $D_{en2E}(s)$ determined by coupling branch in equipment. Both the self-stability path and the interacting path affect frequency stability by affecting the balance between reactive reference current and reactive current feedback.

A. Stability Analysis of PLL Bandwidth's Influence

The parameters of the basic scenario are shown in the appendix. To determine the stability results represented by the positive and negative of $\mathrm{Re}[D(j\omega_m)]$, the slope of $\omega-\mathrm{Im}[D(j\omega)]$ in the basic scenario is analyzed. The result is shown in Fig. 7. $\omega-\mathrm{Im}[D(j\omega)]=0$ is used to estimate the oscillation frequency with high risk of oscillation instability. We can see the slope is greater than 0 when it crosses the horizontal axis, so $\mathrm{Re}[D(j\omega_m)]\leq 0$ means the system is stable. Fig. 8 (a) shows the change curve of $\mathrm{Re}[D(j\omega_m)]$ as the PLL's bandwidth increases, and the horizontal axis represents the multiple of PLL's bandwidth relative to the basic scenario. Obviously, the increase of PLL's bandwidth is adverse to system's stability. Fig. 8 (b) shows the change curve of the dominant oscillation frequency's damping ratio ξ with PLL's bandwidth changes by eigenvalue analysis method, where $\xi>0$ represents the system is stable. It is obvious that $\mathrm{Re}[D(j\omega_m)]$ and ξ have similar trend, so $\mathrm{Re}[D(j\omega_m)]$ can reflect the stability margin well.

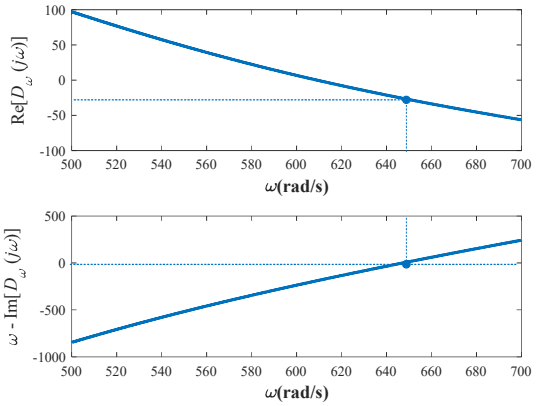

Fig. 7. Stability judgment of basic scenario's system

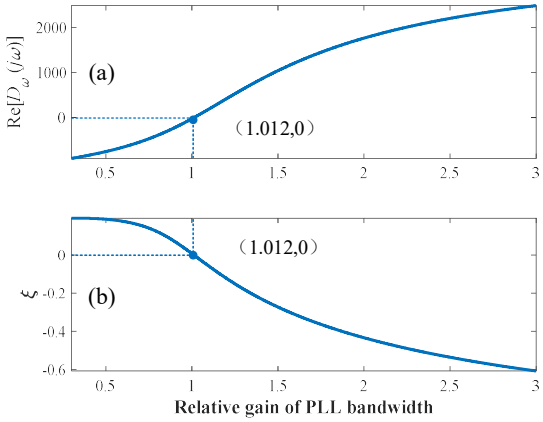

Fig. 8 (a) The change curve of $\mathrm{Re}[D(j\omega_m)]$ with PLL's bandwidth increase;(b) The change curve of ξ with PLL bandwidth increase

To reveal the mechanism of frequency stability from the perspective of the reactive/active currents balancing, Fig.9. shows the change curve of Re[$D_{self1\omega}(s)$], Re[$D_{self2\omega}(s)$], Re[$D_{en1E}(s)$], Re[$D_{en2E}(s)$] with PLL bandwidth increase. Re[$D_{self1\omega}(s)$] increases and changes from negative to positive which indicates that the self-stability of the frequency dynamic through the main branch changes from beneficial to adverse to the frequency stability. Re[$D_{self2\omega}(s)$]<0 and decreases with PLL bandwidth increase, which means the self-stability through the coupling branch in equipment is increasely beneficial to the stability. However, the change range of Re[$D_{self2\omega}(s)$] is smaller than Re[$D_{self1\omega}(s)$], therefore, the frequency dynamic will be increasely adverse to its own stability with PLL's bandwidth increase in general. The mechanism of instability is explained as follows. As shown in Fig. 5, if there is a disturbance such as Δa_ω increases, then $\Delta\omega_e$ increases, after passing through the self-stability path, the unbalanced reactive current's trend changes from decreasing to increasing with PLL bandwidth increases, which in turn makes Δa_ω changes from decreasing to increasing, that is changing from be beneficial for frequency to restore stability to be adverse for frequency restoring stability. Re[$D_{en1E}(s)$] and Re[$D_{en2E}(s)$] are both positive, and increase first and then decrease which indicates that the interaction between amplitude and frequency is adverse to frequency stability. That is $\Delta\omega_e$ increases, the unbalanced reactive current will be increased through the interacting path, which in turn be adverse for frequency restoring stability.

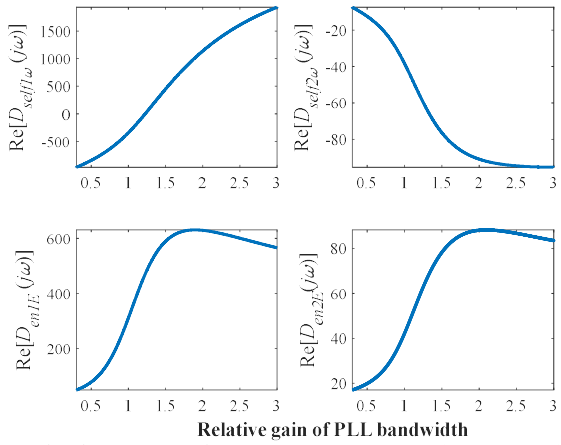

Fig. 9. The change curve of Re[$D_{self1\omega}(s)$], Re[$D_{self2\omega}(s)$], Re[$D_{en1E}(s)$], Re[$D_{en2E}(s)$] with PLL's bandwidth increase

B. Stability Analysis of Current Controller's Influence

Fig. 10 (a) shows the change curve of Re[$D(j\omega_m)$] as the proportional coefficient k_{pcd} of PI regulator in *d* axis increase. It can be seen the increase of k_{pcd} will weaken frequency's stability. Fig.11. shows the change curve of Re[$D_{self1\omega}(s)$], Re[$D_{self2\omega}(s)$], Re[$D_{en1E}(s)$], Re[$D_{en2E}(s)$] with k_{pcd} increase. Re[$D_{self1\omega}(s)$]<0, and increase slightly; Re[$D_{self2\omega}(s)$] changes from positive to negative, so it's easy to find Re[$D_{self\omega}(s)$]<0 and decrease with k_{pcd} increases. That's mean the frequency dynamic is increasely beneficial to its own stability, and mainly affected by the self-stablility path determined by the coupling branch in equipment. Re[$D_{en1E}(s)$]>0, first increases and then decreases slightly, Re[$D_{en2E}(s)$] changes from negative to positive, so it's easy to find Re[$D_{enE}(s)$] increases with k_{pcd} increases and is positive in most time. That is, the interaction between amplitude and frequency is increasingly adverse to the frequency stability. Whereas, the increase of Re[$D_{enE}(s)$] will finally surpass the decrease of Re[$D_{self\omega}(s)$] and lead to frequency instability, which means the unfavorable effect of interaction between amplitude and frequency is greater than the advantageous effect of frequency's self-stability, the system loses stability.

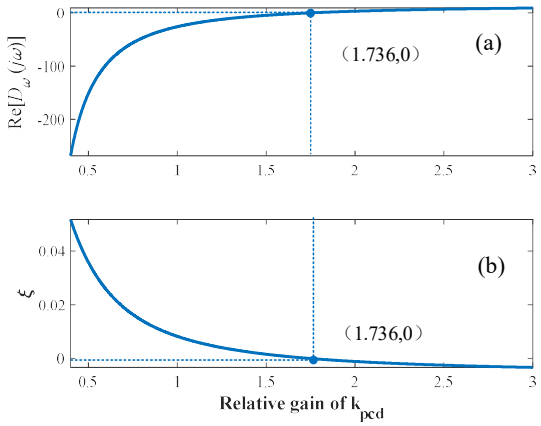

Fig. 10. (a) The change curve of Re[$D(j\omega_m)$] with k_{pcd} increase;(b) The change curve of ξ with k_{pcd} increase

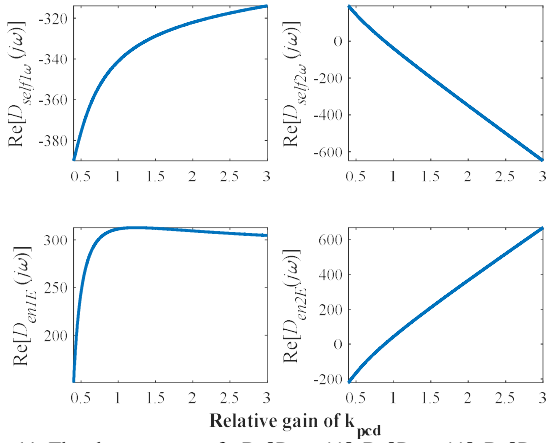

Fig. 11. The change curve of Re[$D_{self1\omega}(s)$], Re[$D_{self2\omega}(s)$], Re[$D_{en1E}(s)$], Re[$D_{en2E}(s)$] with k_{pcd} increase

Fig. 12 (a) shows the change curve of Re[$D(j\omega_m)$] as the proportional coefficient k_{pcq} of PI regulator in *q* axis increases. It can be seen the increase of k_{pcq} will strengthen frequency's stability. Fig.13. shows the change curve of Re[$D_{self1\omega}(s)$], Re[$D_{self2\omega}(s)$], Re[$D_{en1E}(s)$], Re[$D_{en2E}(s)$] with k_{pcq} increases. Re[$D_{self1\omega}(s)$]<0, and increases slightly; Re[$D_{self2\omega}(s)$] changes from negative to positive, so it's easy to find Re[$D_{self\omega}(s)$] changes from negative to positive and is dominated by the change of Re[$D_{self2\omega}(s)$]. That's mean the frequency dynamic is less and less beneficial to its own stability and be adverse finally, and is mainly affected by the

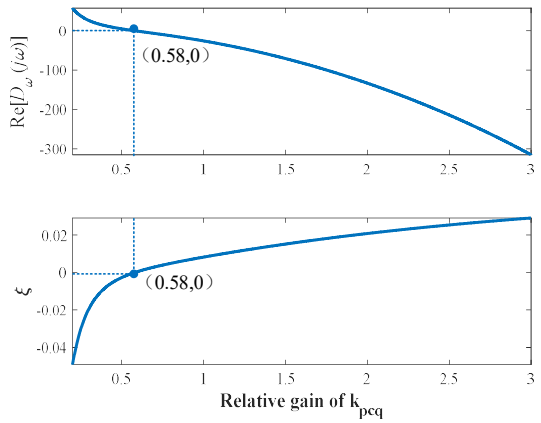

Fig. 12. (a) The change curve of Re[$D(j\omega_m)$] with k_{pcq} increase;(b) The change curve of ξ with k_{pcq} increase

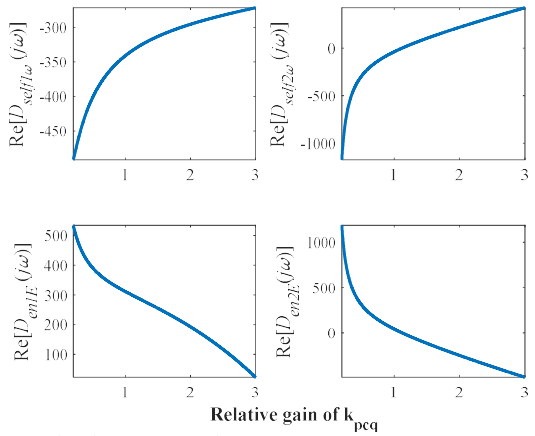

Fig. 13. The change curve of Re[$D_{self1\omega}(s)$], Re[$D_{self2\omega}(s)$], Re[$D_{en1E}(s)$], Re[$D_{en2E}(s)$] with k_{pcq} increase

self-stablility path determined by the coupling branch in equipment. Re[$D_{en1E}(s)$]>0, and decreases with k_{pcq} increase; Re[$D_{en2E}(s)$] changes from positive to negative; it's easy to find Re[$D_{enE}(s)$] changes from positive to negative with k_{pcq} increases. That is, the interaction between amplitude and frequency is less and less adverse to the frequency stability and be beneficial finally. When the unfavorable effect of interaction between amplitude and frequency is less than the advantageous effect of frequency's self-stability, the system becomes stable.

C. Stability Analysis of Terminal Voltage Feedforward's Influence

The higher cut off angle frequency a_{fv} in $F_v(s)$, the more ideal the terminal voltage feedforward is, and according to Fig. 14, the better the frequency stability is. According to Fig. 15, Re[$D_{self1\omega}(s)$] and Re[$D_{self2\omega}(s)$] decrease and change from positive to negative with a_{fv} increase, so frequency dynamic is less and less adverse to the frequency stability and be beneficial finally. Re[$D_{en1E}(s)$] and Re[$D_{en2E}(s)$] increase with a_{fv} increase and change from negative to positive, so the interaction between amplitude and frequency is less and less beneficial to frequency stability and be adverse finally. When the unfavorable effect of interaction between amplitude and frequency is less than the advantageous effect of frequency's self-stability, the system becomes stable.

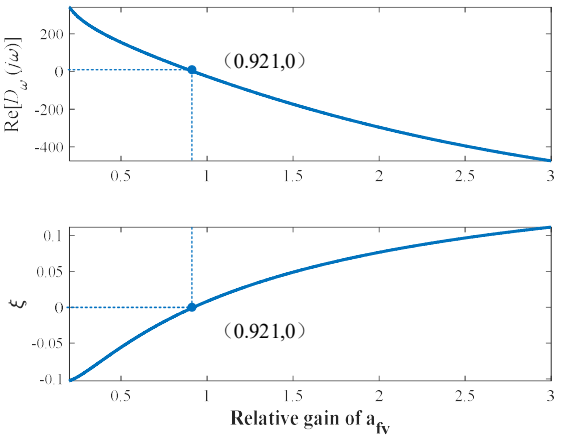

Fig. 14. (a) The change curve of Re[$D(j\omega_m)$] with a_{fv} increase;(b) The change curve of ξ with a_{fv} increase

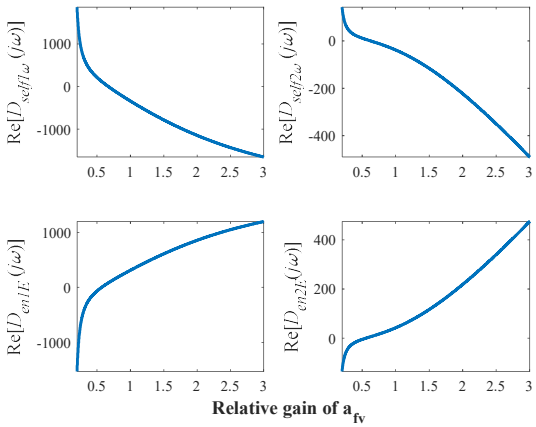

Fig. 15. The change curve of Re[$D_{self1\omega}(s)$], Re[$D_{self2\omega}(s)$], Re[$D_{en1E}(s)$], Re[$D_{en2E}(s)$] with a_{fv} increase

D. Validation by Time Domain

In order to verify the correctness of the above analysis, time domain simulation is carried out in Matlab/Simulink. Fig.16. shows the response curve of VSC's internal voltage phase with PLL bandwidth, k_{pcd}, k_{pcq} and a_{fv} change and the disturbance appears at t=0.5s. Obviously, the increases of PLL bandwidth and k_{pcd} can strength frequency stability; the increase of k_{pcq} and a_{fv} will weaken frequency stability. The simulation results prove the correctness of the above analysis.

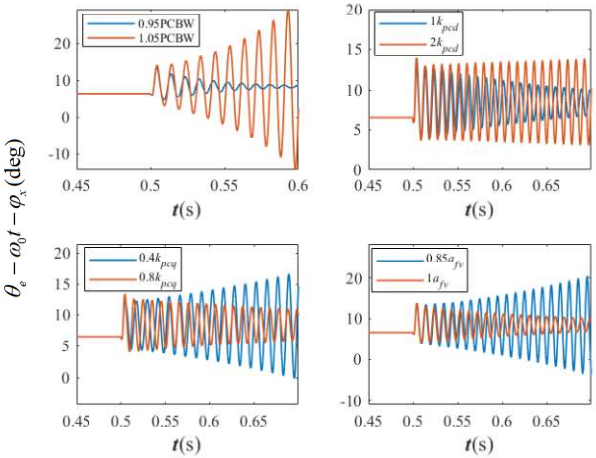

Fig. 16. Response curve of VSC's internal voltage phase with PLL bandwidth, k_{pcd}, k_{pcq} and a_{fv} change.

V. CONCLUSION

This paper establishes a small signal model of VSC considering PLL's dynamic, controller parameter asymmetry in *dq* axis and terminal voltage feedforward based on motion equation concept in CC time-scale, and analyzes the influence of PLL bandwidth, current controller parameters in *dq* axis and filter bandwidth on the stability of the VSC grid-connected system based on a SISO equivalent method which preserves the interaction path between variables in the original MIMO system. The conclusion is as follows: (1) The increase of PLL's bandwidth will weaken the system's stability. The influence of frequency dynamic changes from be beneficial to be adverse to its own stability, and the amplitude dynamic is increasely adverse to the frequency stability. (2) The increase of k_{pcd} will weaken the system's stability. The frequency dynamic is increasely beneficial to its own stability, and the amplitude dynamic is increasingly adverse to the frequency stability. (3) The increase of k_{pcq} will strengthen the system's stability. The frequency

dynamic is less and less beneficial to its own stability, and the amplitude dynamic is less and less adverse to the frequency stability. (4) The increase of a_{fv} will strengthen the system's stability. The frequency dynamic is less and less adverse to its own stability and be beneficial finally, amplitude dynamic is less and less adverse to the frequency stability is less and less beneficial to frequency stability and be adverse finally.

VI. APPENDIX

A. Parameters of the Studied System

S_{base}(kW)	100	R_c(p.u.)	0.55
V_{base}(V)	690	I^p_{dref}, I^p_{qref}	0.8,-0.2
f_{base}(Hz)	50	a_{fv}	1200π
L_f(p.u.)	0.15	PLL:k_{pp},k_{ip}	540,50400
L_g(p.u.)	0.64	k_{pcd},k_{icd}	1.6,64
C_f(p.u.)	0.05	k_{pcq},k_{icq}	1.6,64

B. Specific Expressions of Transfer Functions in the Paper

(1)
$$\begin{cases} G_{dpll}(s)=\dfrac{\left(G_{cq}(s)+sL_f\right)G_p(s)sin\left(\varphi_e-\varphi_p\right)}{1-F_v(s)+sL_fI^p_{d0}G_p(s)} \\ G_{qpll}(s)=\dfrac{\left(G_{cq}(s)+sL_f\right)G_p(s)cos\left(\varphi_e-\varphi_p\right)}{1-F_v(s)+sL_fI^p_{d0}G_p(s)} \end{cases}$$

(2)
$$\begin{cases} G_{Epll}(s)=\dfrac{G_{dpll}(s)G_{\omega q}(s)/s-G_{qpll}(s)G_{\omega d}(s)}{G_{\omega q}(s)G_{Ed}(s)/s/s-G_{Eq}(s)G_{\omega d}(s)} \\ G_{\omega pll}(s)=\dfrac{G_{qpll}(s)G_{Ed}(s)/s-G_{dpll}(s)G_{Eq}(s)}{G_{\omega q}(s)G_{Ed}(s)/s/s-G_{Eq}(s)G_{\omega d}(s)} \end{cases}$$

(3)
$$\begin{cases} G_{Ed}(s)=s\left\{A+\dfrac{F_v(s)}{1-F_v(s)}\left[A+sL_f+G_{dpll}(s)N\right]\right\} \\ G_{Eq}(s)=B+\omega_0L_f+\dfrac{F_v(s)}{1-F_v(s)}\left[B+G_{qpll}(s)N\right] \\ G_{\omega d}(s)=\dfrac{C}{E_0}+G_{dpll}(s)-\omega_0L_f+\dfrac{F_v(s)}{\left(1-F_v(s)\right)E_0}\left[C+G_{dpll}(s)M\right] \\ G_{\omega q}(s)=s\left\{\dfrac{D}{E_0}+G_{qpll}(s)+\dfrac{F_v(s)}{\left(1-F_v(s)\right)E_0}\left[D+sL_f+G_{qpll}(s)M\right]\right\} \end{cases}$$

$$A=G_{cd}(s)cos^2\left(\varphi_e-\varphi_p\right)+G_{cq}(s)sin^2\left(\varphi_e-\varphi_p\right)$$

$$B=C=\left(G_{cq}(s)-G_{cd}(s)\right)sin2\left(\varphi_e-\varphi_p\right)/2$$

$$D=G_{cq}(s)cos^2\left(\varphi_e-\varphi_p\right)+G_{cd}(s)sin^2\left(\varphi_e-\varphi_p\right)$$

$$M=-sL_fI^p_{q0}sin\left(\varphi_e-\varphi_p\right)-sL_fI^p_{d0}cos\left(\varphi_e-\varphi_p\right)$$

$$N=sL_fI^p_{q0}cos\left(\varphi_e-\varphi_p\right)-sL_fI^p_{d0}sin\left(\varphi_e-\varphi_p\right)$$

(4)
$$\begin{aligned} H_{dE}(s)&=-G_{Epll}(s)I^e_{q0} \\ H_{d\omega}(s)&=-G_{\omega pll}(s)I^e_{q0}+I^e_{q0} \\ H_{qE}(s)&=G_{Epll}(s)I^e_{d0} \\ H_{q\omega}(s)&=G_{\omega pll}(s)I^e_{d0}-I^e_{d0} \end{aligned}$$

VII. REFERENCES

[1] M. Zhao, X. Yuan, and J. Hu, "Voltage Dynamics of Current Control Time-Scale in a VSC-Connected Weak Grid," *IEEE Trans. Power Systems,* vol. 31, pp. 2925-2937, July 2016.

[2] C. Buchhagen, C. Rauscher, and A. Menze "BorWin1 - First Experiences with harmonic interactions in converter dominated grids," presented at the Int. ETG Congress. Die Energiewende - Blueprints for the new energy age, Bonn, Germany, 2015, pp. 1-7.

[3] Y. Wang, X. Wang, F. Blaabjerg and Z. Chen, "Harmonic Instability Assessment Using State-Space Modeling and Participation Analysis in Inverter-Fed Power Systems," *IEEE Trans. Industrial Electronics*, vol. 64, pp. 806-816, Jan. 2017.

[4] M. Cespedes and J. Sun, "Impedance Modeling and Analysis of Grid-Connected Voltage-Source Converters," *IEEE Trans. Power Electronics*, vol. 29, pp. 1254-1261, March 2014.

[5] A. Rygg, M. Molinas, C. Zhang and X. Cai, "A Modified Sequence-Domain Impedance Definition and Its Equivalence to the dq-Domain Impedance Definition for the Stability Analysis of AC Power Electronic Systems," *IEEE Journal of Emerging and Selected Topics. Power Electronics*, vol. 4, pp. 1383-1396, Dec. 2016.

[6] B. Wen, D. Boroyevich, and R. Burgos, "Analysis of D-Q Small-Signal Impedance of Grid-Tied Inverters," *IEEE Trans. Power Electronics*, vol.31,pp.675-687, Dec.2015.

[7] L. Xu, H. Xin, and L. Huang, "Symmetric Admittance Modeling for Stability Analysis of Grid-Connected Converters," *IEEE Trans. Energy Conversion*, vol. 35, pp. 434-444, March 2020.

[8] S. Li, Y. Yan and X. Yuan, "SISO Equivalent of MIMO VSC-Dominated Power Systems for Voltage Amplitude and Phase Dynamic Analyses in Current Control Timescale," *IEEE Trans. Energy Conversion*, vol. 34, pp. 1454-1465, Sept. 2019.

[9] S. Li, M. Zhang and X. Yuan, "A method for multi-VSC interaction analysis based on current excitation and voltage response in current control timescale," presented at the 8th RPG. Conf. Shanghai, China, 2019.

[10] H. Liu, X. Xie and W. Liu, "An Oscillatory Stability Criterion Based on the Unified dq -Frame Impedance Network Model for Power Systems With High-Penetration Renewables," IEEE Trans. Power Systems, vol. 33, pp. 3472-3485, May 2018.

VIIII. BIOGRAPHIES

Yaxin Peng was born in China. He received the B.Eng. degree in electrical engineering and automation from Wuhan University, Wuhan, China, in 2018. She is currently working toward the M.Eng. degree in electrical engineering at Huazhong University of Science and Technology, Wuhan, China. His research interests include modeling of voltage source converter and stability analysis.

Xiaoming Yuan was born in China. He received the B.Eng. degree from Shandong University, China, the M.Eng. degree from Zhejiang University, China, and the Ph.D degree from Federal University of Santa Catarina, Brazil, in 1986,1993,and 1998 respectively, all in electrical engineering. He was with Qilu Petrochemical Corporation, China, from 1986 to 1990, where he was involved in the commissioning and testing of relaying and automation devices in power systems, adjustable speed drives, and high-power UPS systems. From 1998 to 2001, he was a Project Engineer at the Swiss Federal Institute of Technology Zurich, Switzerland, where he worked on flexible-ac-transmission-systems and power quality. From 2001 to 2008, he was with GE GRC shanghai as a Manager of the Low Power Electronics Laboratory. From 2008 to 2010, he was with GE GRC US as an Electrical Chief Engineer. His research field involves stability and control of power system with multimachines multiconverters, control and grid-integration of renewable energy generations, and control of high voltage dc transmission systems. Dr.Yuan is a Distinguished Expert of the National Thousand Talents Program of China, and the Chief Scientist of the National Basic Research Program of China(973 Program).He received the first prize paper award from the Industrial Power Converter Committee of the IEEE industry Applications Society in 1999.